

***Ab initio* investigation of lithium on the diamond C(100) surface**K. M. O'Donnell,^{1,2,*} T. L. Martin,^{2,3} N. A. Fox,³ and D. Cherns³¹*The Bristol Centre for Nanoscience and Quantum Information, University of Bristol, Bristol BS8 1FD, United Kingdom*²*School of Chemistry, University of Bristol, Bristol BS8 1TS, United Kingdom*³*Department of Physics, H. H. Wills Physics Laboratory, University of Bristol, Bristol BS8 1TH, United Kingdom*

(Received 2 July 2010; published 7 September 2010)

We have performed *ab initio* calculations to investigate the adsorption of Li onto the clean and oxygenated diamond C(100) surface. Despite a large amount of interest in alkali-metal absorption on clean and oxidized semiconductor surfaces for both fundamental and technological applications, lithium adsorption on the diamond surface has not been reported. We find that Li adopts structures on the clean C(100) surface similar to those reported for Na, K, and Rb on diamond, though Li exhibits significantly higher binding energies in the range 2.7–3.1 eV per Li adsorbate. For the oxygenated C(100)-(1 × 1):O surface, the lowest energy involving a full Li monolayer structure shows an exceptionally large work-function shift of −4.52 eV relative to the clean surface, an effect similar to that seen for Cs—O on diamond, but with a higher binding energy of 4.7 eV per Li atom. We propose that such a system, if verified by experiment, is suitable for the surface coating of diamond-based vacuum electronic devices, as it should exhibit higher thermal stability than the commonly used Cs—O surface while retaining the advantage of a large lowering of the work function.

DOI: [10.1103/PhysRevB.82.115303](https://doi.org/10.1103/PhysRevB.82.115303)

PACS number(s): 73.30.+y, 73.20.At, 68.43.Bc, 73.20.Hb

I. INTRODUCTION

Diamond is a promising photocathode, field emitter, and thermionic emitter due to its chemical stability, high thermal conductivity, and the relative ease of inducing a negative electron affinity. A negative electron affinity, where the conduction-band minimum is at a higher energy than the vacuum level, is invariably induced by a surface treatment leading to an adsorbate^{1–4} or thin-film structure^{5–7} on the diamond surface. For electron emission applications, a caesium submonolayer adsorbed on the oxygenated diamond surface has been investigated extensively due to the extremely low work function induced by the large Cs—O dipole, reducing the work function of the bare diamond surface from 5.5–6 eV to around 1.25 eV.^{3,4,8,9} The caesium layer is relatively stable in air⁹ but cannot withstand temperatures in excess of approximately 400 °C, too low for thermionic applications.³ As such, research into diamond thermionics has focused on the use of hydrogen termination, which is known to induce a negative electron affinity (NEA) of around −1 eV for a number of crystallographic planes of diamond.¹⁰ Hydrogen has been observed¹ to evolve from the monohydride-terminated surface between 740–900 °C, which is an acceptable upper bound for diamond thermionic converters currently of interest for solar power generation and heat recycling. The dipole generated by hydrogen on the diamond surface is, however, rather small, leading to measured work functions in the range 2.85–3.9 eV.^{2,10} For low-temperature thermionic applications, work functions near 1 eV are desirable. Hence, thermally stable but highly polar surface structures are of interest.

Reported alternatives to hydrogen for inducing a NEA on diamond include thin metal films,¹¹ alkali-metal monolayers,¹² alkali-halide films,^{5,13} and alkali-oxide monolayers such as the aforementioned CsO coatings. The alkali metals feature prominently because of the strong polar bonds they form with other elements. Wong *et al.*, investigated the

work-function reduction due to thin films of lithium fluoride⁵ and rubidium fluoride.¹³ In the case of lithium fluoride, a relatively thick film of 15 Å reduces the work function of the (100) diamond surface to 2.4 eV, whereas rubidium fluoride requires a film of just 2 Å to reduce the work function to the range 2.0–2.5 eV. Potassium adsorption has been investigated by Petrick and Benndorf,¹² who report low sticking coefficients on the hydrogen-terminated diamond (100) surface but near-unity adsorption for an oxygen-terminated surface, strong evidence of the need for charge transfer and dipole formation in alkali-metal adsorption on diamond. Similarly, caesium is found to adsorb strongly on oxygenated diamond but not on the bare surface.³

Alkali-metal adsorption on silicon and germanium has been the subject of a large number of experiments for more than three decades with considerable disagreement in the literature regarding adsorption sites and saturation coverages. Early experimental work showed a complex adsorption series inferred from low-energy electron-diffraction (LEED) images.¹⁴ Although Levine's early work on Cs adsorption on Si(100) suggested that saturation coverage was reached at 0.5 monolayers (MLs),¹⁵ later experiments indicated that full monolayer coverage could be reached for smaller alkali metals via a “double-layer” structure on Si(100) for K at least.^{16–18} More recent measurements appear to validate the 0.5 ML coverage limit for Cs.¹⁹ We should note that there is variation in the literature as to what constitutes a monolayer on a dimerized surface such as C(100), Si(100), or Ge(100). Due to the reconstruction of such surfaces into dimer rows, there are two atoms per unit cell, making the traditional definition of a monolayer-one adsorbate atom per surface atom-less suitable. Some authors prefer the convention that one monolayer equals one adsorbate per dimer, others use one adsorbate per unit cell. Here we use the latter-one monolayer corresponds to one adsorbate per 1 × 1 cell, or equivalently, one adsorbate per top layer atom. In many studies of Si and Ge, alkali metals are used in conjunction with oxygen adsorption.^{15,20,21} The work-function changes induced by

oxygenation suggest that oxygen plays a role in modifying the surface dipoles created by alkali-metal adsorption. Similar effects have been observed on diamond surfaces,^{4,12,22} motivating us to examine the lightest alkali metal, lithium, on diamond surfaces, on the basis that it should form stronger bonds with diamond than heavier alkali metals while still reducing the work function.

Lithium adsorption on silicon has been the subject of both computational^{23–25} and experimental^{17,26,27} studies, however to the best of our knowledge, lithium adsorption on diamond has not been reported. It is generally found that up to a coverage of approximately 1 ML, Li adsorbs on Si in a similar fashion to hydrogen rather than at the Levine sites observed for the heavier alkali metals. At higher coverages, there is evidence that a silicide is formed. Both structures are distinct even from the next lightest alkali metal, sodium, and suggest a size effect is at play.¹⁷ On this basis it is difficult to single out any analogous system for lithium adsorption on diamond, and therefore in the present work we make comparison with a range of systems on both diamond and silicon.

Lithium is widely used in organic light-emitting diodes and polymer solar-cell fabrication as a work-function-lowering interface material and electron injector, and as a result thin films are easily produced *in situ* using commercially available dispenser technology. It is therefore a potential practical candidate for inducing a low-work-function surface for vacuum microelectronic applications, particularly thermionic converters based on NEA diamond. In this paper, we report what we believe are the first *ab initio* calculations for lithium adsorbed onto the C(100)-(2×1) and C(100)-(1×1):O surfaces. The properties of Li adsorption on diamond are found to be in general agreement with heavier alkali metals on diamond, silicon, and germanium. The most interesting result however, is that for the most tightly bound system consisting of a full monolayer of Li adsorbed onto a fully oxygenated C(100) surface, the calculations yield a large negative electron affinity and high binding energy per Li atom.

II. COMPUTATIONAL DETAILS

Plane-wave density-functional theory (DFT) calculations were made using the CASTEP program²⁸ on the BlueCrystal Phase 2 high-performance computing cluster at the University of Bristol. The Perdew and Wang (PW91) functional²⁹ was used as the generalized gradient approximation to the exchange-correlation functional. Ultrasoft Vanderbilt pseudopotentials³⁰ were used for each of the atomic species of C, Li, H, and O considered in the present work. The pseudopotentials give bulk lattice constants for diamond and lithium of 3.57 Å and 3.46 Å, respectively, within 1.5% of the experimental values of 3.560 Å (Ref. 31) and 3.511 Å.³² A plane-wave cutoff energy of 700 eV was used for all simulations. The C(100) surface was modeled using a double-sided thick slab geometry with 22 layers of C atoms, approximately 21 Å of vacuum gap between opposing faces and simulation cell dimensions of 5.05 Å×2.52 Å×42.84 Å. The cell was oriented to give a single 2×1 dimer unit on each end of the

slab and two carbon atoms per layer. The cell dimensions were kept fixed during the calculation, using the lattice constant of 3.57 Å obtained from a separate calculation on a conventional eight-atom diamond unit cell. The double-sided slab geometry was used to ensure that the electric field decayed to zero between the two faces so that accurate work-function calculations could be made. A Monkhorst-Pack grid³³ of 6×6×1 *k* points was found sufficient for the structural calculations while 12×12×1 *k* points were used for the density-of-states (DOS) calculations. For each structure, the geometry was optimized with a fixed unit cell via the Broyden, Fletcher, Goldfarb, and Shannon method with a convergence criterion of 0.02 eV/Å. No atomic positions were constrained during the geometry optimization. Adsorption energies are calculated as

$$E_{ads} = (E_{substrate} + NE_{atom} - E_{tot})/N, \quad (1)$$

where E_{tot} is the total calculated energy for the adsorbed surface, $E_{substrate}$ is the total energy of the preadsorbed surface, N is the number of adsorbate atoms in the simulation cell, and E_{atom} is the total energy of the individual adsorbate calculated from the species pseudopotential. The adsorption energies are positive for stable adsorption.

Work functions were calculated using the macroscopic averaging method of Fall, Binnig, and Baldereschi.³⁴ First, a large 3×3 conventional unit-cell bulk calculation involving 216 carbon atoms in the diamond structure was used to calculate the bulk Fermi level $E_{f,b}$ and hence the difference between $E_{f,b}$ and the plane-averaged mean electrostatic potential in the bulk, $\tilde{V}_{es,b}$,

$$\Delta E = E_{f,b} - \tilde{V}_{es,b} = 10.52 \text{ eV}. \quad (2)$$

The difference was then added to the mean electrostatic potential within the slab to find the appropriate Fermi level for the slab $E_{f,s}$. The difference between the mean vacuum level in the vacuum gap region E_{vac} and the slab Fermi level gives the work function,

$$\phi = E_{vac} - E_{f,s} = E_{vac} - \tilde{V}_{es,s} + \Delta E. \quad (3)$$

The same method using the full local potential including exchange/correlation led to essentially identical physical quantities, most likely because of the large vacuum gap and symmetric geometry leading to a reliable vacuum level. The electron affinity χ was calculated by subtracting the vacuum level from the conduction-band minimum, taken as the slab Fermi level plus the experimental diamond band gap of 5.47 eV.³⁵

III. RESULTS

A. Base structures

There are a number of experimental and theoretical reports of the structure of clean, annealed and hydrogen/oxygen terminated (100) diamond that can be used to check our methodology. The principal experimental studies are the investigation of the electron affinity of the C(100) surface by Maier³⁶ and Baumann.¹ The clean, unreconstructed C(100)

TABLE I. Key structural and electronic properties for the clean, hydrogenated, and oxygenated diamond (100) surfaces, compared to other theoretical findings.

Structure	Source	E_{abs} (eV)	χ (eV)	$d_{11(C-C)}$ (Å)	d_{CO} (Å)	d_{CH} (Å)
C(100)-(2×1)	Present work	1.46 ^a	0.62	1.38		
	Prev. DFT	1.512 (Ref. 39)	0.51–0.69 (Ref. 45), 0.8 (Ref. 46)	1.37 (Ref. 40)		
C(100)-(2×1):2H	Present work	5.32	−1.95	1.62		1.10
	Prev. DFT	4.54 (Ref. 40)	−2.0 (Ref. 45), −2.2 (Ref. 46)	1.61 (Ref. 40)		1.11 (Ref. 47), 1.1 (Ref. 40)
C(100)-(1×1):O (ether)	Present work	8.2	2.63	No dimer	1.50	
	Prev. DFT	8.43 (Ref. 43)	2.61–2.70 (Ref. 45)	No dimer	1.48 (Ref. 42), 1.49 (Ref. 43)	
C(100)-(1×1):O (carbonyl)	Present work	7.88	3.75	No dimer	1.20	
	Prev. DFT	8.57 (Ref. 43)	3.64 (Ref. 45)	No dimer	1.25 (Ref. 43), 1.16 (Ref. 42)	

^aPer surface atom relative to the unreconstructed surface.

surface has two dangling electrons per surface atom, leading to a large number of structural possibilities. Freshly grown chemical-vapor deposition diamond surfaces tend to be monohydride terminated. The monohydride surface exhibits a 2×1 LEED pattern³⁷ consistent with the formation of single C—H bonds on top of a reconstructed symmetric dimer row structure.^{38–40} Natural or high-pressure, high-temperature synthetic diamonds have a mix of hydrogen and oxygen terminations. Oxygen can attach to the C(100) surface in a number of ways, generally showing a 1×1 LEED pattern.^{41–43} The carbonyl (or ketone) structure, consisting of a double bond between carbon and oxygen above every surface site, has been calculated to be slightly higher in energy than the ether bridging structure where oxygen atoms bond between and across atomic sites. A high-temperature anneal can be used to remove both hydrogen and oxygen, leaving a clean 2×1 reconstructed surface. Hydrogen is reported⁴⁴ to begin to leave the surface at approximately 740 °C and be completely absent (after a suitable annealing time) between 900–1050 °C, whereas Auger electron spectroscopy results¹ continue to show an oxygen peak until above 1050–1100 °C.

Our *ab initio* results for these basic structures appear in Table I, showing the dimer and adsorbate bond lengths, adsorption energies per adatom and electron affinity. Note that we refer to the monohydride surface as C(100)-(2×1):2H as there are two hydrogen atoms per surface unit cell. The associated structures appear in Fig. 1. The results generally agree very well with other theoretical results with the exception of the adsorption energies, which are more strongly affected by the method of computation. For the clean C(100)- 2×1 surface we find a work function of 6.1 eV, leading to a small positive electron affinity of 0.6 eV, consistent with the experimental findings of 0.75 eV by Baumann¹ and 0.50 eV by Maier.³⁶ Our values are also consistent with those calculated by Robertson⁴⁵ and van der Weide.⁴⁶ The positive electron affinity is consistent with the strong dimer double bond for the clean surface giving an increased electron density in the top layer compared to sub-surface layers.

Placing atomic hydrogen above the dimer sites optimises to the same 2×1 monohydride structure obtained if the hydrogen is placed above the surface atoms of the unreconstructed surface. The underlying dimer bond length increases upon hydrogen adsorption, consistent with the transfer of electrons from the double carbon-carbon bond to individual carbon-hydrogen bonds. The hydrogen termination layer reduces the work function of diamond to 3.5 eV, in reasonable agreement with the experimental result of 3.9 eV,⁴⁸ and leads to an electron affinity of −1.95 eV. Such an NEA value agrees fairly well with the experimental results of Maier,³⁶ though we note that it seems generally the theoretical calculations tend to be more negative than experiment.

For the oxygen-terminated surfaces, both carbonyl and ether bridge bonding configurations are found to be stable with bond lengths consistent with their bonding type. We

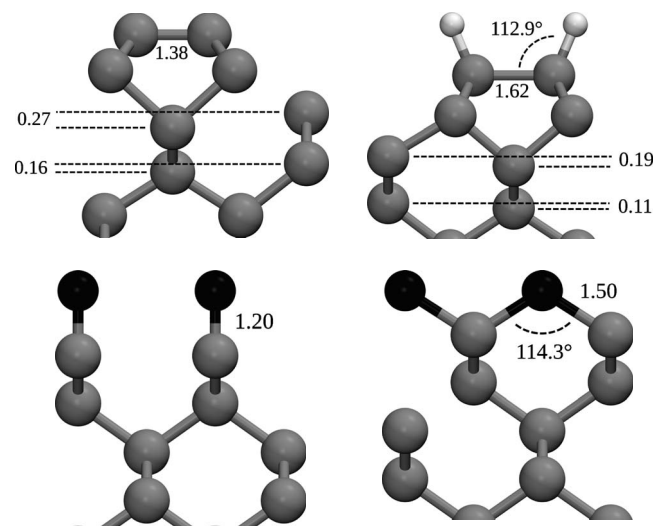


FIG. 1. The optimized structures for (a) C(100)-(2×1), (b) C(100)-(2×1):2H, (c) C(100)-(1×1):O, carbonyl, and (d) C(100)-(1×1):O, ether. Length units are in angstroms.

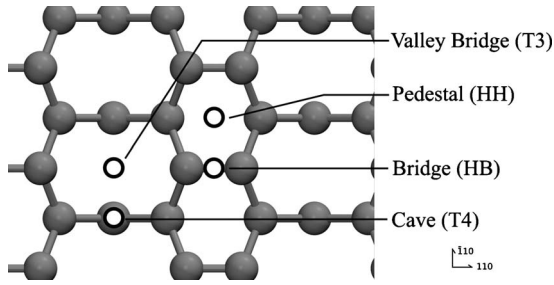


FIG. 2. High symmetry adsorption sites considered for Li adsorption in the present study.

find the ether bond structure is slightly lower in energy by 0.32 eV, agreeing with other DFT studies^{45,49} but theoretical results using other methods show some variance based on the surface lattice parameter used and the oxygen coverage.^{42,43} We note that our results suggest that a full monolayer coverage of oxygen in either structure induces a very large positive electron affinity ranging from 2.63 eV for the ether bridge structure to 3.75 eV for the carbonyl structure. These values agree well with the calculations of Rutter and Robertson.⁴⁵ It is not clear whether the reported experimental values^{1,36} of 1.7 and 1.45 eV are due to ether, ketone, or mixed coverage, though both are significantly less than all the calculated results. It was speculated by Maier³⁶ that some of the difference between experimental and theoretical values of the electron affinity may be at least partly due to incomplete coverage layers of the adsorbate under investigation, particularly for oxygen coverage.

B. Lithium on the clean C(100) surface

We first consider adsorption of lithium onto the clean and reconstructed C(100)-(2×1) surface. Figure 2 shows the sites suggested by previous authors^{25,50} as the most likely adsorption sites for alkali metals on the Si(100) surface, called pedestal (HH), bridge (HB), valley-bridge (T3), and cave (T4) sites. The exact site of adsorption for 0.5 ML for the various alkali metals on Si(100) and Ge(100) has been the subject of much debate, as has the possibility of double-layer adsorption leading to 1 ML coverage.^{16,19,51–55} The Levine sites suggested for silicon have been proposed by others as the likely adsorption sites for alkali-metal species on diamond^{56–58} and these are the locally stable sites found in the present work. Our adsorption energies, bond lengths, calculated work functions, and electron affinities for lithium adsorption at these sites appear in Table II, with associated lowest energy structures in Fig. 3.

For 0.5 ML adsorption, we find that the T3 valley-bridge position is the lowest in energy, the pedestal and cave positions are higher energy but very similar to each other, and the bridge position is the highest energy. The same energy variation is found for K and Rb on Ge(100),⁵⁴ but not for Na, though the differences are small enough to be accounted for by variations in computational method and simulation parameters. Likewise, the order of the adsorption energies for Li on C(100) is generally different to those calculated for Na on Si(100), which might otherwise be considered an analo-

TABLE II. Calculated structural and electronic properties of the Li-adsorbed C(100)-(2×1) surface.

Coverage (ML)	Site	E_{abs} (eV/ads)	$d_{111(C-C)}$ (Å)	d_{C-Li} (Å)	$\Delta\phi$ (eV)	χ (eV)
0.5	T3	3.10	1.52	2.22	-2.07	-1.45
	HH	2.63	1.53	2.13	-3.21	-2.59
	T4	2.57	1.51	2.10	-2.54	-1.92
	HB	2.12	1.46	2.21	-1.77	-1.15
1	HH+T3	3.26	1.74	2.10	-3.32	-2.70
	HH+T4	3.04	1.68	2.10	-3.15	-2.53
	HB+T3	3.02	1.72	2.01	-3.29	-2.67
	HB+T4	2.74	1.64	2.04	-2.99	-2.37

gous system.^{16,51,53} For diamond surfaces, our results are consistent with those of Nie *et al.*^{57,58} who found that Na, K, and Rb preferred valley bridge adsorption. When Li is adsorbed, the dimer bond is longer (1.46–1.53 Å) than the clean reconstructed dimer bond (1.38 Å) which is consistent with a more single-bond character. A projection onto the atomic orbitals of lithium suggests there is Li $2s/2p$ hybridization. For the preferred T3 adsorption site, each Li atom gains a charge of approximately +0.8e. Both the first and second layer carbon atoms gain negative charge in response. The combination of these properties supports a polar covalent interpretation similar to that inferred experimentally by Johansson¹⁷ and Tikhov⁵² for alkali metals on Si(100).

Like hydrogen, the adsorption of lithium is predicted to significantly reduce the diamond work function and induce a negative electron affinity. For a 0.5 ML coverage of Li, the most stable valley-bridge position gives a work function shift of -2.07 eV which is significantly smaller than the values calculated by Nie *et al.* for Na, K, and Rb adsorption.^{57,58} We suggest that the larger size of the heavier alkali metals leads to a larger induced dipole per adsorption site.

For 1 ML coverage of Li, our results suggest that the HH-T3 combination is slightly favored over the alternative

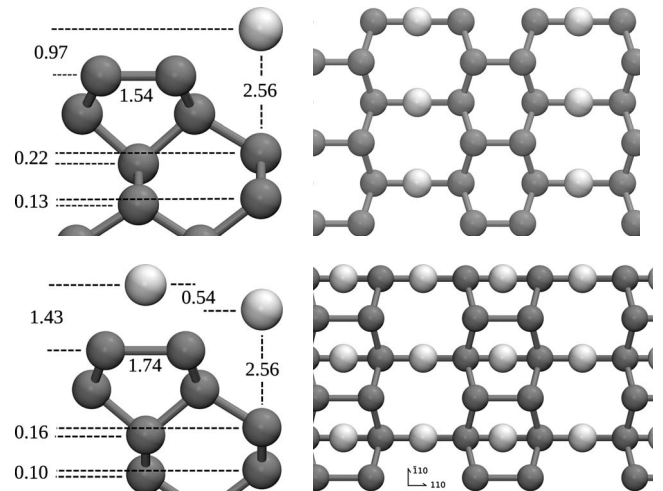


FIG. 3. Lowest energy structures in section and plan views for [(a) and (b)] 0.5 ML and [(c) and (d)] 1 ML Li adsorption on C(100)-(2×1).

TABLE III. Structural and electronic properties for lithium adsorption on the C(100)-(1×1):O surface.

Coverage (ML)	Structure	E_{abs} (eV/ads)	d_{CO} (Å)	$d_{11(C-C)}$ (Å)	d_{Li-O} (Å)	$\Delta\phi$ (eV)	χ (eV)
0.5	OP	4.71 (K), 4.07 (E)	1.27	No dimer	1.87	-2.70	-2.08
	OB	3.54 (K)	1.25	No dimer	1.74	-1.87	-1.25
1	HH+T3	4.70 (K), 4.38 (E)	1.40	1.65	1.81, 1.86	-4.52	-3.89
	HB+T3	3.90 (K), 3.76 (E)	1.36	1.66	1.67, 1.86	-3.00	-2.38
	HB+T4	3.36 (K)	1.35	1.62	1.67, 1.75	-2.30	-1.67

combinations shown in Table II. The HH-T3 combination appears to be generally favored for double-layer models that accommodate 1 ML adsorption.^{51,54,59} The important result here is that our adsorption energies per atom for the 1 ML system are approximately the same or larger than those for the 0.5 ML case. It would appear Li on C(100) is an extreme case of the observation by Johansson¹⁷ that smaller alkali metals have stronger adsorbate-substrate binding and weaker adsorbate-adsorbate interactions. Computed values for larger alkali metals on C(100) partially agree with the trend. For example, Nie *et al.*⁵⁷ give a 24% reduction in adsorption energy per adsorbate going from 0.5 to 1 ML Na coverage on C(100) and a 75% reduction for a similar change of K coverage. We note that their calculations for Rb (Ref. 58) do not follow this trend, and further, other structural parameters such as the dimer bond length do not monotonically vary with alkali-metal size.

We find that the work-function shift as a function of Li coverage does not show the prominent minima at 0.5 ML predicted for Na and K. In fact, for 1 ML of Li in the HB-T3 combination, the work-function shift for the full coverage is more than 1 eV greater than the sum of the shifts caused by the individual 0.5 ML coverages of Li in the bridge or valley-bridge positions. Similarly, for the energetically favorable HH-T3 combination, the work-function shift of the full monolayer is larger than that of the constituent 0.5 ML. From this we conclude that dipole depolarization is not significant for the Li-adsorbed surface at these coverages, in contrast to the heavier alkali metals. On the other hand, the monotonic decrease in the work function with increasing lithium concentration is consistent with the calculations for Na on Si(100),⁶⁰ suggesting again that a size effect is responsible for the difference between Li and the other alkali metals on diamond. Efforts are underway to locate the exact work-function minimum as a function of increasing coverage.

Electronically, all the optimized structures predict a negative electron affinity for Li adsorbed on C(100)-(2×1), varying from -1.15 to -2.7 eV. The two lowest energy configurations give negative electron affinities of -1.45 and -2.7 eV for 0.5 ML and 1 ML of Li, respectively. These values are comparable to the values obtained for hydrogen adsorption, although the Li adsorbates are less strongly bound, and for practical use a “sticking” layer is likely to be necessary. For this reason we have investigated the adsorption of Li onto oxygenated diamond surfaces in analogy with previous experimental work showing the sticking coefficient for alkali metals on diamond is much higher when the surface is oxygen terminated.¹²

C. Lithium on C(100)-(1×1):O

The symmetry of the (1×1):O surface termination on diamond (100) reduces the number of distinct high symmetry sites shown in Fig. 2 to two: the HB and T4 sites of the clean surface become equivalent, as do the HH and T3 sites. We denote these two unique sites the oxygen bridge position (OB), where the lithium adsorbate has two O nearest neighbors, and the oxygen pedestal position (OP), where it has four O neighbors. Carbon dimer rows form for full monolayer coverage and hence for the monolayer case we use the standard positions of HH, HB, T3, and T4. Finally, since computational results tend to place the ether (bridge) and ketone (carbonyl) oxygen bonding structures very close in energy, we have investigated Li adsorption for both cases. However, in some cases the resulting final structure is identical. For simplicity we present only the stable, unique structures, with adsorption energies for adsorption on ketone and ether bonded surfaces suffixed by K and E, respectively, when appropriate. Our calculated results appear in Table III.

Figure 4 shows the lowest energy structures for 0.5 and 1 ML coverage of Li on C(100)-(1×1):O. The lowest energy structure occurs where each oxygen sits vertically over a single carbon atom and Li sits in the pedestal site over the oxygen monolayer. As might be expected, the surface potential landscape for ether-bonded diamond seems considerably

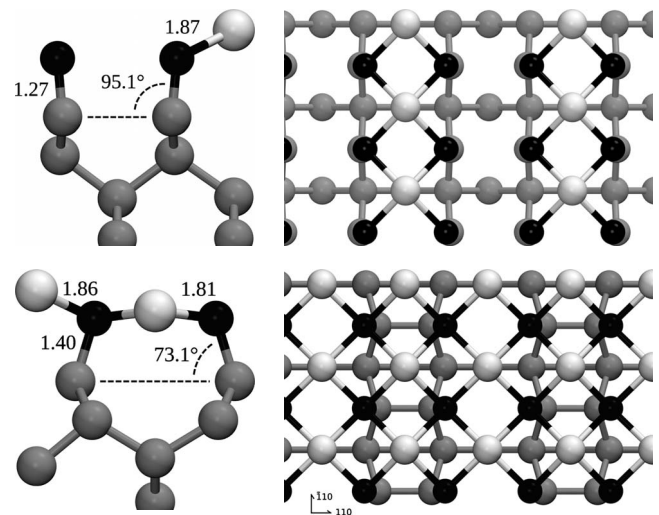


FIG. 4. Lowest energy structures in section and plan views for [(a) and (b)] 0.5 ML and [(c) and (d)] 1 ML Li adsorption on C(100)-(1×1):O.

more complex than that of the clean reconstructed diamond surface. For example, the OB-adsorbed structure on the ether-bonded surface appears not to be a local minimum and results in a highly asymmetric structure with both C—O bonds canted in the same direction. The carbon-oxygen bond for the OP/OB adsorbed, ketone-bonded surface changes only slightly, with a small decrease in bond population and increase in bond length. However Li adsorption at the OP site breaks the bridge structure of the ether-bonded surface and yields the same final configuration as for the ketone-bonded surface.

For 1 ML Li adsorption, there are three unique Li adsorption site pairs; the pedestal-valley-bridge (HH-T3), bridge-valley-bridge (HB-T3), and bridge-cave (HB-T4) pairs, to adapt the terminology used earlier. On the ketone-bonded oxygen surface, all three adsorption site pairs lead to unique structures, with the HH-T3 structure having the lowest energy overall, as seen with Li adsorption on the clean surface. On the ether-bonded structure, stable 1 ML coverage again requires the C—O—C bridges to be broken to form vertical C—O bonds similar to that observed for the 0.5 ML pedestal-site adsorption. This only occurred for the HH-T3 and HB-T3 configurations. The final state in each of these is identical to that found for HH-T3 and HB-T3 adsorption on the ketone-bonded surface. Attempting to optimize the HB-T4 configuration in the ether structure always resulted in the Li atoms moving away from the surface.

The lowest energy structure, the HH-T3 monolayer, has a binding energy of 4.7 eV per Li atom, which is comparable to hydrogen adsorption on the clean diamond surface (5.3 eV per H atom) and much higher than that calculated for Cs on oxygenated diamond⁸ (1.34 eV per Cs atom). The binding energy per Li for 1 ML is almost identical to that for 0.5 ML, indicating interaction between the Li atoms on the surface is minimal, as found for adsorption on the clean surface earlier. The most interesting feature of the surface is that there is a very large work-function shift of -4.52 eV. In our calculation, the average potential in the bulk is -5.9 eV, with the vacuum level at 6.2 eV. Adding 10.52 eV to the average potential gives the Fermi level for the slab, which lies approximately 1.6 eV below the vacuum level and yields an electron affinity of -3.9 eV. Although caesiated oxygen terminated surfaces are predicted to have lower work functions down to 1.25 eV, the Li monolayer structure suggested here is more strongly bound and more useful for higher-temperature applications.

The adsorption of Li to 1 ML into the HH and T3 positions forces a slight reconstruction of the oxygen monolayer and the first layer carbon. Unlike the 0.5 ML case, the carbon-oxygen bonds take on a more single-bonded character and the first layer of carbon atoms dimerize but with a much larger dimer bond length of 1.65 Å compared to the usual 1.38 Å of the clean surface, consistent with a single bond. The surface unit cell is therefore very nearly (but not exactly) a (1×1) structure with a LiO basis. Therefore, for simplicity we henceforth refer to this structure as C(100)- (1×1) :LiO. Each oxygen atom is surrounded by four lithium atoms, reminiscent of the structure suggested by Parker and Rhead⁶¹ for the adsorption of oxygen on lithium-coated Ag(111).

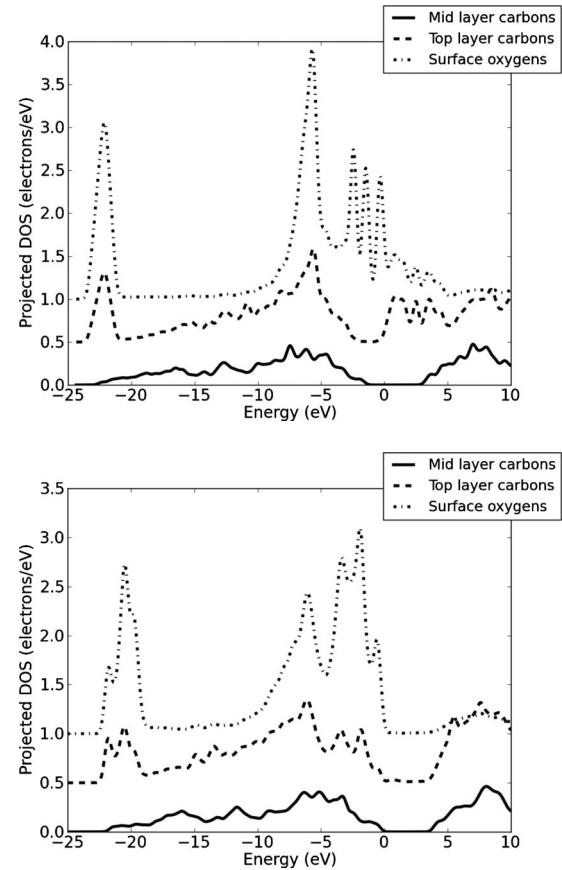


FIG. 5. (a) PDOS for bulk C, surface C, and surface O prior to Li adsorption on the C(100)- (1×1) :O surface. (b) The PDOS for the same layers after 1 ML Li adsorption. All energies are relative to the Fermi level at 0 eV. Individual graphs have been shifted vertically for clarity.

A more careful examination of the bonding is warranted to determine the distribution of electron density that gives rise to the surface dipole. Consider the DOS projected onto surface oxygen, first layer carbon and midlayer carbon atoms as shown in Fig. 5, for the C(100)- (1×1) :O and C(100)- (1×1) :LiO structures. For the surface without lithium in Fig. 5(a), the midlayer carbons have broad features indicative of sp^3 character as would be expected for diamond, while the first layer carbon atoms have increased sp^2 character matching with the oxygen states. The lone-pair levels for oxygen appear as sharp, nonbonding peaks mostly within the band gap. The projected DOS (PDOS) structure is very similar to that calculated by Zheng *et al.*,⁶² though in their case the lone-pair levels appear to be more closely spaced. In contrast to the oxygenated surface, the projected DOS for the C(100)- (1×1) :LiO structure in Fig. 5(b) shows the oxygen lone pair levels significantly shifted down in energy giving overlap with the bulk levels, apparently allowing delocalization (as evidenced by the broadening) and a general shift of negative charge away from the surface. The downshift in the oxygen electron energies is consistent with the presence of the positive Li^+ ion and bonding of an ionic character. The atomic population for Li indicates partial hybridization with 0.27–0.31 electrons in the $2p$ states. In the present case, the ionic bonds appear to be reducing the en-

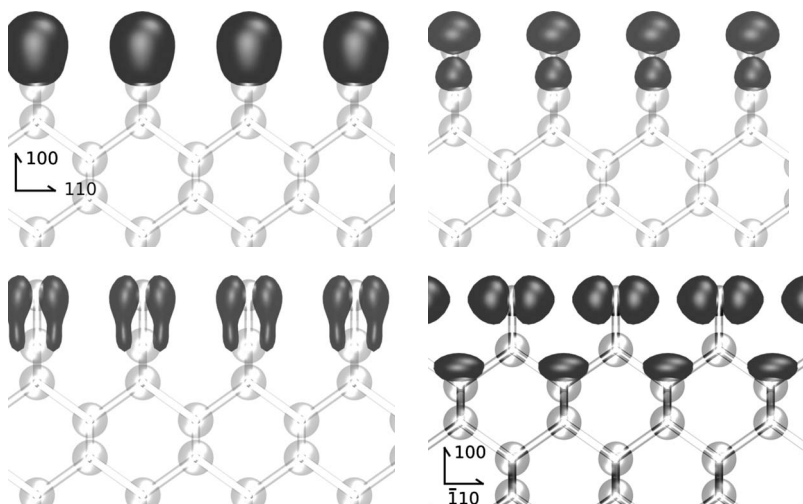


FIG. 6. Sum of Kohn-Sham densities for the localized orbitals in the C(100)-(1×1):O system. (a) σ -like bonds with band energies around -22 eV relative to the Fermi level. (b) sp -like bonds with band energies near -6 eV. (c) π -like bonds with band energies in the range -5 to -2 eV. (d) p-shaped orbitals with energies near -2.44 , -1.47 , and 0.34 eV. Note the orientation change in (d).

ergy of the surface enough to remove the occupied band gap states.

It is natural to consider how the electron density for these upper level states shifts upon Li adsorption onto the oxygenated surface. Although the Kohn-Sham orbitals do not represent single-electron bonds, it has been suggested that they are at least as useful as other approximate molecular orbitals^{63,64} to generate a bonding perspective and have been used a great deal for visualization in quantum chemistry. Figure 6 shows the sum of electron densities generated by the Kohn-Sham eigenstates for a particular subset of bands for the C(100)-(1×1):O system. Each group of bands corresponds to a set of strongly localized orbitals with p-like, π -like, or σ -like shapes, as might be expected for conventional C=O bonding. For example, the bands giving the electron density in Fig. 6(d) are the six highest Kohn-Sham occupied eigenstates. These states have energies near -2.44 , -1.47 , and -0.34 eV relative to the Fermi level, and hence it can be seen that they are the source of the sharply peaked states in Fig. 5(a).

For the C(100)-(1×1):LiO surface, only the two highest-energy occupied bands show significant localization above the delocalized levels [Fig. 7(a)]. Further, each of the two bands are localized on opposite faces of our model slab, thus physically there are only two surface-localized electrons near the Fermi level per surface unit cell. The remaining occupied bands near the Fermi level show delocalization over at least the first few atomic layers of the substrate [Fig. 7(b)] as expected from the corresponding projected density of states in Fig. 5(b). Instead of isolated bands leading to distinctive bonding shapes between the top atomic layers, the higher-energy occupied bands that correspond to lone pairs for the C(100)-(1×1):O surface tend to show charge distributed

across the upper layers for the C(100)-(1×1):LiO surface. We suggest that these effects account for what must be a significant dipole effect in shifting the work function by -4.52 eV. The viewpoint we propose here may be applicable to other systems such as Na on Si(100) or K on Ge(100), however, we note that for the large alkali metals such as Cs, a more conventional dipole model based on atomic centers has been applied with some success for both C(100) and Si(100).¹⁴ We should also make clear that we are not suggesting Li and O are coadsorbed to the surface carbons in the sense of Albano.⁶⁵ The central reason the present case differs from previous work is that Li appears to accommodate into the oxygenated surface system without serious structural distortion, leading to a different electronic effect than that observed for the heavier alkali metals. For example, for Cs on oxygenated diamond, Pickett⁸ has shown that repulsion between the Cs $5p$ semicore states and C—O bonding states is a contributing factor to the surface dipole, whereas in the case of Li, the core $1s$ states are much lower in energy than those of the lattice and should not interact.

Finally, we should make clear here that these calculations have been made for intrinsic diamond only, and do not include the effects of band bending induced by the presence of dopants and surface defects, which is why we have emphasized the work-function shift for the adsorbates rather than the absolute work function. In electron emission applications, it is likely that a doping diamond substrate would be needed for practical devices. Nevertheless, the present study suggests that the C(100)-(1×1):LiO system is a good candidate for the active surface of such devices due to the high binding energy of the adsorbate and the large work-function shift induced by lithium adsorption.

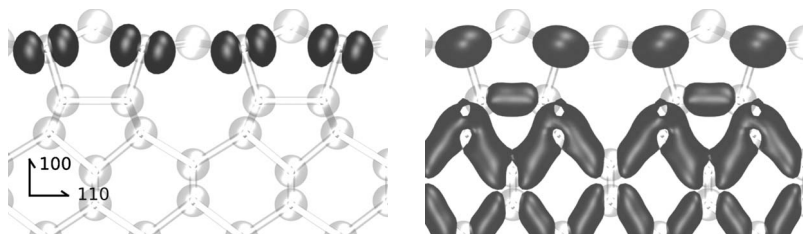


FIG. 7. (a) The sole localized orbitals (one electron per surface oxygen) for the C(100)-(1×1):LiO surface with band energies in the range -0.4 to -2.0 eV. (b) The remaining orbitals near the Fermi level are delocalized.

IV. CONCLUSIONS

We have performed *ab initio* calculations for Li adsorption on the clean C(100)-(2×1) and C(100)-(1×1):O surfaces. We find that on the clean surfaces, the preferred adsorption sites agree with those generally agreed as the preferred adsorption sites for other alkali metals, and that the work-function shifts are consistent with those calculated and observed for alkali metals such as Na and K on diamond. We find the binding energy for Li adsorbed layers to be higher for Li than those reported for Na, K, and Rb. Our observation of monotonically decreasing work function as the coverage changes from 0 to 0.5 to 1 ML agrees with calculations for the structurally similar Na on Si(100) system but contrasts with the calculated results for Na, K, and Rb on diamond. For the oxygenated C(100)-(1×1):O surface we find Li adsorption appears to require either that the oxygen surface structure has a ketone C=O character or that C—O—C bridge bonds are broken such that the underlying oxygen monolayer has a single oxygen above each carbon. The binding energies of Li to the oxygenated surface are much higher than the binding energies of Li to the bare surface, and are large enough to be competitive with hydrogen as an active surface for diamond electron emitters. We cal-

culate that the energetically preferred structure for 1 ML coverage has a binding energy of 4.7 eV per lithium atom and yields a large work-function shift of approximately −4.52 eV with a negative electron affinity of −3.9 eV. Our calculations suggest that Li adsorption leads to partial delocalization of charges that would otherwise be bound tightly to the surface, leading to a large effective dipole. Based on the large work-function shifts and strong binding energies we propose that the 1 ML Li on C(100)-(1×1):O system is a possible candidate for low work-function applications, in particular, field and thermionic emission devices.

ACKNOWLEDGMENTS

This report is based on a project which was funded by E.ON AG as part the E.ON International Research Initiative. Computational work was carried out using the computational facilities of the Advanced Computing Research Centre, University of Bristol—<http://www.bris.ac.uk/acrc/>. K.O.D. would like to thank Mike Ashfold and Neil Allan for constructive feedback and Ben Truscott for valuable technical advice.

*kane.odonnell@bristol.ac.uk

- ¹P. Baumann and R. J. Nemanich, *Surf. Sci.* **409**, 320 (1998).
- ²L. Diederich, O. Küttel, P. Aebi, E. Maillard-Schaller, R. Fasel, and L. Schalpabach, *Diamond Relat. Mater.* **7**, 660 (1998).
- ³K. P. Loh, J. S. Foord, R. G. Egdell, and R. B. Jackman, *Diamond Relat. Mater.* **6**, 874 (1997).
- ⁴K. Loh, X. Xie, S. Yang, J. Pan, and P. Wu, *Diamond Relat. Mater.* **11**, 1379 (2002).
- ⁵K. W. Wong, Y. Wang, K. Lee, and R. Kwok, *Diamond Relat. Mater.* **8**, 1885 (1999).
- ⁶F. Köck, J. Garguilo, B. Brown, and R. J. Nemanich, *Diamond Relat. Mater.* **11**, 774 (2002).
- ⁷P. Baumann and R. J. Nemanich, *Appl. Surf. Sci.* **104-105**, 267 (1996).
- ⁸W. E. Pickett, *Phys. Rev. Lett.* **73**, 1664 (1994).
- ⁹M. Geis, J. Twichell, J. Macaulay, and K. Okano, *Appl. Phys. Lett.* **67**, 1328 (1995).
- ¹⁰L. Diederich, P. Aebi, O. Küttel, and L. Schalpabach, *Surf. Sci.* **424**, L314 (1999).
- ¹¹P. Baumann and R. J. Nemanich, *J. Appl. Phys.* **83**, 2072 (1998).
- ¹²S. Petrick and C. Benndorf, *Diamond Relat. Mater.* **10**, 519 (2001).
- ¹³K. Wong, Y. Wang, S. Lee, and R. Kwok, *Appl. Surf. Sci.* **140**, 144 (1999).
- ¹⁴R. Holtom and P. Gundry, *Surf. Sci.* **63**, 263 (1977).
- ¹⁵J. Levine, *Surf. Sci.* **34**, 90 (1973).
- ¹⁶T. Urano, K. Sakaue, K. Nagano, S. Hongo, and T. Kanaji, *J. Cryst. Growth* **115**, 411 (1991).
- ¹⁷L. S. O. Johansson and B. Reihl, *Surf. Sci.* **287-288**, 524 (1993).
- ¹⁸S. Tanaka, N. Takagi, N. Minami, and M. Nishijima, *Phys. Rev. B* **42**, 1868 (1990).
- ¹⁹W. B. Sherman, R. Banerjee, N. J. DiNardo, and W. R. Graham, *Phys. Rev. B* **62**, 4545 (2000).
- ²⁰J. E. Ortega, E. M. Oellig, J. Ferrón, and R. Miranda, *Phys. Rev. B* **36**, 6213 (1987).
- ²¹D. Edwards, *Appl. Surf. Sci.* **1**, 419 (1978).
- ²²O. Küttel, O. Gröning, E. Schaller, L. Diederich, P. Gröning, and L. Schalpabach, *Diamond Relat. Mater.* **5**, 807 (1996).
- ²³H. Q. Shi, M. W. Radny, and P. V. Smith, *Phys. Rev. B* **69**, 235328 (2004).
- ²⁴H. Shi, M. Radny, and P. Smith, *Surf. Sci.* **574**, 233 (2005).
- ²⁵Y. Morikawa, K. Kobayashi, and K. Terakura, *Surf. Sci.* **283**, 377 (1993).
- ²⁶M. K. J. Johansson, S. M. Gray, and L. S. O. Johansson, *Phys. Rev. B* **53**, 1362 (1996).
- ²⁷K. Shin, C. Kim, and J. Chung, *Appl. Phys. A* **60**, 35 (1995).
- ²⁸S. Clark, M. Segall, C. Pickard, P. Hasnip, M. Probert, K. Refson, and M. Payne, *Z. Kristallogr.* **220**, 567 (2005).
- ²⁹J. P. Perdew and Y. Wang, *Phys. Rev. B* **46**, 12947 (1992).
- ³⁰D. Vanderbilt, *Phys. Rev. B* **41**, 7892 (1990).
- ³¹D. Rilby, *Nature (London)* **153**, 587 (1944).
- ³²E. Covington and D. Montgomery, *J. Chem. Phys.* **27**, 1030 (1957).
- ³³H. Monkhorst and J. Pack, *Phys. Rev. B* **13**, 5188 (1976).
- ³⁴C. Fall, N. Binggeli, and A. Baldereschi, *J. Phys.: Condens. Matter* **11**, 2689 (1999).
- ³⁵C. Clark, P. Dean, and P. Harris, *Proc. R. Soc. London, Ser. A* **277**, 312 (1964).
- ³⁶F. Maier, J. Ristein, and L. Ley, *Phys. Rev. B* **64**, 165411 (2001).
- ³⁷L. Ley, R. Graupner, J. Cui, and J. Ristein, *Carbon* **37**, 793 (1999).
- ³⁸Z. Jing and J. Whitten, *Surf. Sci.* **314**, 300 (1994).
- ³⁹J. Furthmüller, J. Hafner, and G. Kresse, *Europhys. Lett.* **28**, 659 (1995).

- (1994).
- ⁴⁰J. Furthmüller, J. Hafner, and G. Kresse, *Phys. Rev. B* **53**, 7334 (1996).
- ⁴¹J. Ristein, *Surf. Sci.* **600**, 3677 (2006).
- ⁴²H. Tamura, H. Zhou, K. Sugisako, Y. Yokoi, S. Takami, M. Kubo, K. Teraishi, A. Miyamoto, A. Imamura, M. N.-Gamo, and T. Ando, *Phys. Rev. B* **61**, 11025 (2000).
- ⁴³X. Zheng and P. Smith, *Surf. Sci.* **262**, 219 (1992).
- ⁴⁴M. Kataoka, C. Zhu, F. A. M. Koeck, and R. J. Nemanich, *Diamond Relat. Mater.* **19**, 110 (2010).
- ⁴⁵M. J. Rutter and J. Robertson, *Phys. Rev. B* **57**, 9241 (1998).
- ⁴⁶J. van der Weide, Z. Zhang, P. K. Baumann, M. G. Wensell, J. Bernholc, and R. J. Nemanich, *Phys. Rev. B* **50**, 5803 (1994).
- ⁴⁷Y. Yang and M. D'Evelyn, *J. Vac. Sci. Technol. A* **10**, 978 (1992).
- ⁴⁸L. Diederich, O. Küttel, P. Aebi, and L. Schalpabach, *Surf. Sci.* **418**, 219 (1998).
- ⁴⁹S. J. Sque, R. Jones, and P. R. Briddon, *Phys. Rev. B* **73**, 085313 (2006).
- ⁵⁰T. Abukawa and S. Kono, *Phys. Rev. B* **37**, 9097 (1988).
- ⁵¹P. Krüger and J. Pollmann, *Appl. Phys. A* **59**, 487 (1994).
- ⁵²M. Tikhov, G. Boishin, and L. Surnev, *Surf. Sci.* **241**, 103 (1991).
- ⁵³L. Spiess, P. Mangat, S. Tang, K. Schirm, A. Freeman, and P. Soukiassian, *Surf. Sci. Lett.* **289**, L631 (1993).
- ⁵⁴H. Xiao, X. Zu, Y. Zhang, and F. Gao, *Chem. Phys. Lett.* **417**, 6 (2006).
- ⁵⁵B. Czech, P. Mikołajczyk, and B. Stankiewicz, *Appl. Surf. Sci.* **256**, 4784 (2010).
- ⁵⁶M. Hossain, T. Kubo, T. Aruga, N. Takagi, T. Tsuno, N. Fujimori, and M. Nishijima, *Diamond Relat. Mater.* **9**, 162 (2000).
- ⁵⁷J. L. Nie, H. Xiao, X. Zu, and F. Gao, *Chem. Phys.* **326**, 308 (2006).
- ⁵⁸J. L. Nie, H. Xiao, X. Zu, and F. Gao, *Physica B* **383**, 219 (2006).
- ⁵⁹Y. Morikawa, K. Kobayashi, K. Terakura, and S. Blügel, *Phys. Rev. B* **44**, 3459 (1991).
- ⁶⁰K. Kobayashi, Y. Morikawa, K. Terakura, and S. Blügel, *Phys. Rev. B* **45**, 3469 (1992).
- ⁶¹S. Parker and G. Rhead, *Surf. Sci.* **167**, 271 (1986).
- ⁶²J. Zheng, X. Xie, A. Wee, and K. Loh, *Diamond Relat. Mater.* **10**, 500 (2001).
- ⁶³E. Baerends and O. Gritsenko, *J. Phys. Chem. A* **101**, 5383 (1997).
- ⁶⁴R. Stowasser and R. Hoffmann, *J. Am. Chem. Soc.* **121**, 3414 (1999).
- ⁶⁵E. Albano, *Appl. Surf. Sci.* **14**, 183 (1983).